HHS Public Access

Author manuscript

Neuron. Author manuscript; available in PMC 2016 May 02.

Published in final edited form as:

Neuron. 2008 June 12; 58(5): 763–774. doi:10.1016/j.neuron.2008.03.030.

High-Frequency Network Oscillations in Cerebellar Cortex

Steven J. Middleton[1,4], **Claudia Racca**[1], **Mark O. Cunningham**[1], **Roger D. Traub**[2], **Hannah Monyer**[3], **Thomas Knöpfel**[4], **Ian S. Schofield**[5], **Alistair Jenkins**[5], and **Miles A. Whittington**[1,*]

[1]Institute of Neuroscience, The Medical School, Newcastle University, Newcastle upon Tyne, NE2 4HH, UK

[2]Departments of Physiology, Pharmacology, and Neurology, SUNY Downstate Medical Center, Brooklyn, NY 11203, USA

[3]Department of Clinical Neurobiology, University Hospital of Neurology, IZN, Im Neuenheimer Feld 364, 69120 Heidelberg, Germany

[4]Laboratory for Neuronal Circuit Dynamics, RIKEN Brain Science Institute, 2-1 Hirosawa, Wako-shi, Saitama 351-0198, Japan

[5]Regional Neurosciences Center, Newcastle General Hospital, Newcastle upon Tyne, NE7 7DN, UK

SUMMARY

Both cerebellum and neocortex receive input from the somatosensory system. Interaction between these regions has been proposed to underpin the correct selection and execution of motor commands, but it is not clear how such interactions occur. In neocortex, inputs give rise to population rhythms, providing a spatiotemporal coding strategy for inputs and consequent outputs. Here, we show that similar patterns of rhythm generation occur in cerebellum during nicotinic receptor subtype activation. Both gamma oscillations (30–80 Hz) and very fast oscillations (VFOs, 80–160 Hz) were generated by intrinsic cerebellar cortical circuitry in the absence of functional glutamatergic connections. As in neocortex, gamma rhythms were dependent on $GABA_A$ receptor-mediated inhibition, whereas VFOs required only nonsynaptically connected intercellular networks. The ability of cerebellar cortex to generate population rhythms within the same frequency bands as neocortex suggests that they act as a common spatiotemporal code within which corticocerebellar dialog may occur.

INTRODUCTION

Somatosensory information is processed at multiple levels in the central nervous system. Two of the principal areas involved in interpreting such information are the somatosensory neocortex and the sensorimotor areas of the cerebellum. In neocortex, sensory input is temporally organized by concurrently generated rhythms at a range of frequencies. In particular, rhythms in the classical gamma band (30–80 Hz) and higher (very fast oscillations, or “high gamma” rhythms) have been shown to be involved in coding for

*Correspondence: m.a.whittington@ncl.ac.uk.

various features of sensory stimuli (Gray et al., 1989; Womelsdorf et al., 2007; Canolty et al., 2006). In human neocortex, somatosensory stimuli evoke gamma rhythms in somatosensory cortex (Palva et al., 2005). The dynamic synchronization of these gamma rhythms is linked to precision sensorimotor tasks (Tecchio et al., 2007) and selective attention to tactile stimuli (Bauer et al., 2006). More specifically, event-related synchronization at gamma frequencies is related to the onset and execution of motor commands (Szurhaj et al., 2005). In general, the classical gamma rhythm appears to function as a temporal code in cortex, facilitating the dynamic formation of neuronal assemblies (Harris et al., 2003) by permitting synchronous firing among multiple, spatially separate subpopulations of neurons (Gray et al., 1989; Fries, 2005). Higher-frequency rhythms, up to 150 Hz, are also seen in neocortex in response to sensory input. These very fast oscillations (VFOs) are temporally correlated with activity in the gamma band and have been suggested to be a more precise indicator of neocortical response to input (Canolty et al., 2006).

In cerebellar cortex, much less is known about oscillatory responses to somatosensory stimulation. Corticocerebellar coherence at gamma frequencies is seen in monkeys during manual precision grip tasks (Soteropoulos and Baker, 2006), and cerebellothalamic activity is synchronized with neocortical activity at gamma frequencies (Timofeev and Steriade, 1997). Within cerebellum, Purkinje cell synchronization is associated with transition from rapid, tonic firing to more temporally correlated discharges with periods of around 20 ms (within the classical gamma band; Shin and De Schutter, 2006). However, activity within the VFO range is commonly observed in cerebellar recordings (Niedermeyer, 2004), but its function is, as yet, unknown.

A similar discrepancy exists when considering evidence for underlying mechanisms of gamma and VFO activity in somatosensory neocortex and cerebellar cortex. Gamma rhythms in neocortex are predominantly interneuron mediated, with cortical principal cell firing under powerful control via phasic perisomatic $GABA_A$ receptor-mediated inhibitory potentials (Whittington et al., 1995; Cunningham et al., 2004). Local and distal feedback circuits exist to provide inhibitory interneurons with fast glutamatergic synaptic excitation, which, in turn, generates coherent interneuronal spiking to provide this gamma frequency principal cell input. The dynamic interplay between local and distal principal cell/interneuron connections provides an ideal template for synchronization of neuronal outputs over a range of spatial scales limited only by axonal conduction delays (Traub et al., 1996; Kopell et al., 2000). In addition to these synaptic mechanisms, neocortical gamma rhythms are critically dependent on direct electrical communication between neurons mediated by gap junctions (Cunningham et al., 2004). It is proposed that gap junctional communication between electrically active subcompartments of neurons provides a background network drive nested within the classical gamma rhythm (Traub et al., 2003). When studied in isolation, gap junctionally connected networks generate field potential rhythms in the VFO range (Draguhn et al., 1998; Schmitz et al., 2001)—such frequencies are seen independently of GABAergic inhibition in rat somatosensory cortex in vivo (Jones and Barth, 2002).

Given that both neocortex and cerebellum are activated by somatosensory stimuli, we tested the hypothesis that the cerebellum is also capable of generating gamma and VFO rhythms in vitro and found that this is the case. Analysis revealed both similarities and clear differences.

Despite differences in their underlying mechanisms, cerebellar cortex was able to generate population rhythms within the same frequency bands as neocortex, suggesting that these rhythms act as a common spatiotemporal code facilitating dialog between these brain areas.

RESULTS

Pharmacological Induction of Cerebellar Cortical High-Frequency Oscillations

In hippocampal and neocortical brain slices that lack physiological input, local network oscillations can be readily induced with the anticholinesterase physostigmine. The appearance of oscillations following reduction of the breakdown of endogenously released acetylcholine implies the presence of functional cholinergic terminals in these structures. The resulting gamma rhythms are generated via muscarinic acetylcholine receptor activation (Fisahn et al., 1998; A. Roopun and M.A.W., unpublished data). To test whether a similar mechanism exists in cerebellar cortex, where cholinergic inputs originate from various subcortical regions, such as the pedunculopontine tegmental nucleus (Jaarsma et al., 1997), we bath applied 10 μM physostigmine and observed both gamma and VFO rhythms occurring persistently (>3 hr) in field recordings from the Purkinje cell layer. The gamma band activity had a peak modal frequency of 43 ± 2 Hz (n = 6) and median power of 1659 (IQR 1603 → 2212) μV^2 ($p < 0.05$, Figure 1A). In addition, a smaller peak in the field power spectrum indicated the generation of VFO rhythms with mean frequency in the range 80–170 Hz. In contrast to neocortex and hippocampus, the muscarinic receptor antagonist atropine (10 μ.M) had no significant effect on either component of the spectrum ($p > 0.1$, n = 5, data not shown). However, the physostigmine-induced population oscillation was replicated entirely by bath application of 2–20 μM nicotine (Figure 1B). Nicotine (10 μM) produced oscillations with a principal peak frequency of 42 ± 1 Hz (n = 9) and a smaller peak in the VFO range (80 ± 3 Hz). Power in the gamma band was 657 ± 77 μV^2 following application of nicotine ($p < 0.001$). In native slices, no frequency bands were observed. It should be noted that oscillations could not be generated in sagittal cerebellar slices, with no significant changes observed in either mean gamma or VFO area powers following physostigmine ($p > 0.5$, n = 5) or nicotine ($p > 0.5$, n = 5) application. All areas of the cerebellar hemispheres and vermis were systematically tested for the occurrence of oscillatory activity. However, in the presence of nicotine, crus I and II of the ansiform and paramedian lobules were the only areas that generated oscillatory activity (data not shown).

Immunoreactivity for nicotinic acetylcholine receptor subunits α_3. α_4, α_6, α_7, β_2, and β_4 is found in human cerebellum (Graham et al., 2002). With the exception of the α_6 subunit, these subunits are also seen in rodent cerebellum (Quik et al., 2000; Yeh et al., 2001). We therefore used nicotinic antagonists with a range of subunit selectivities to attempt to elucidate the identity of receptors involved in rhythm generation. Prior to application, the stable gamma frequency oscillations had a mean gamma band area power of 1066 ± 114 μV^2. Following addition of the broad-spectrum nicotinic receptor antagonist d-tubocurarine (dTC, 10 μM), the modal peak frequency in the spectrum (representing the gamma frequency activity) was significantly reduced (mean gamma band area power 140 ± 66.3 μV^2) (Figure 1C, $p < 0.001$, n = 5). In addition, the VFO was abolished upon treatment of d-tubocurarine, with mean area power being reduced from 2334 ± 163 μV^2 to 126 ± 46.7 μV^2

($p < 0.001$, n = 5, paired t test). Classic central nervous system nicotinic receptors were targeted by chlorisondamine diiodide (CDI). CDI (10 μM) had no significant effect on the power of the existing nicotine-induced gamma frequency oscillation (Figure 1C, $p > 0.05$, n = 6), nor did it effect the frequency (39.1 ± 1.91 Hz to 41.4 ± 2.11 Hz, $p > 0.05$, n = 6).

β_2 nicotinic-containing receptors have been shown by Quik et al. (2000) to exhibit a high expression throughout the cerebellum, while to a lesser extent the α_4 and α_7 subunits are also sparsely expressed in adult rodents. However, the $\alpha_4\beta_2$-containing receptor antagonist dihydro-β-erythroidine hydrobromide (DHE, 10 μM) did not significantly affect the nicotine-induced rhythm (control power 812 ± 48.3 μV^2, with DHE 795 ± 49.2 μV^2, $p > 0.05$, n = 6, Figure 1C). In addition, the selective antagonist for α_7-containing neuronal nicotinic receptors, methyllycaconitine citrate (MLA, 10 μM), also had no effect on the nicotine-induced rhythm (control power 821 ± 43.5 μV^2, MLA 864 ± 64.8 μV^2, $p > 0.05$, n = 6). Nicotinic receptors of the type found at neuromuscular junctions have been shown to be functional in the cerebellum (de la Garza et al., 1987). We therefore tested the neuromuscular nicotinic receptor antagonist pancuronium dibromide (pan, 10 μM) and found an incomplete but significant reduction in high-frequency oscillations (control power 607 ± 27.1 μV^2, with pan 454 ± 16.4 μV^2, $p < 0.05$, n = 6, Figure 1C).

Involvement of Synaptic Inhibition

In sharp contrast to local circuits in neocortex, the principal output neurons of cerebellar cortex, the Purkinje cells, are GABAergic. These neurons interact with more conventional local circuit, GABAergic inhibitory interneurons to generate cerebellar output, leading to the possibility that the high-frequency oscillations observed may be generated entirely by networks of inhibitory neurons—a phenomenon observed in hippocampus and neocortex only in nonphysiological conditions (Whittington et al., 1995). To exclude any involvement of fast glutamatergic synaptic activation by granule cells, we applied the AMPA/kainate receptor antagonist NBQX (10 μM), which had no significant effect on nicotine-induced high-frequency oscillations (control gamma power 546 ± 93 μV^2, NBQX548 ± 88 μV^2, $p > 0.05$, n = 5, Figure 1D). The VFO component of the high-frequency oscillation was also not significantly affected (control power 627 ± 146 μV^2, NBQX 621 ± 152 μV^2, $p > 0.05$, n = 5). Granule cells also activate molecular layer interneurons via NMDA receptors. However, the NMDA receptor antagonist D-AP5 (50 μM) had no significant effect on gamma or VFO rhythms. Control gamma band area power was 692 ± 73 μV^2 and remained unchanged after D-AP5 application (712 ± 82 μV^2, $p > 0.05$, n = 5, Figure 1E). NMDA receptor blockade also had no significant effect on the VFO induced by nicotine ($p > 0.05$, n = 5).

These data demonstrated that persistent high-frequency oscillations in cerebellum were not generated using mechanisms implicated in hippocampal and neocortical gamma rhythms, where fast glutamatergic synaptic transmission is necessary (Traub et al., 2000; Cunningham et al., 2004). However, $GABA_A$ receptor-mediated inhibition played as crucial a role in cerebellar as in cerebrocortical rhythmogenesis (e.g., Whittington and Traub, 2003). Bath application of gabazine (1 μM) abolished modal spectral peaks in the field gamma band in all cases (n = 5, Figure 2A). However, in contrast to hippocampus, where GABA receptor

activation boosts field VFO oscillations (Traub et al., 2003), in cerebellar slices, gabazine markedly enhanced VFO power (from 263 ± 27 μV^2 to 1659 ± 182 μV^2, n = 5, $p < 0.001$).

As in neocortex, the above data indicated a critical role for $GABA_A$ receptors in generating cerebellar gamma rhythms. To understand the significance of $GABA_A$ergic synaptic transmission, we performed intracellular recordings from Purkinje neurons. Spike rates in control, nonoscillating conditions were 44 ± 4 Hz (n = 7) (Figure 2B) and decreased during nicotine-induced rhythmic activity to 6 ± 1 Hz ($p < 0.001$). This decrease in output was associated with a significant hyperpolarization of mean membrane potential (65 ± 1 mV compared to control levels of 58 ± 1 mV, $p < 0.001$, n = 7). During the high-frequency field potential rhythms (gamma and VFO), Purkinje cells also displayed fast prepotentials (spikelets), which are studied in more detail below. Depolarization of Purkinje cells, to 30 mV, revealed characteristic trains of rhythmic gamma frequency IPSPs in the presence of nicotine, matching the modal peak frequency of the oscillation (42 ± 1 Hz, n = 6) and phase locked, along with full action potentials, to it—as seen with gamma rhythms in cerebral cortical regions.

Involvement of Nonsynaptic Networks in Cerebellar Cortex

The coexistence of gamma rhythms and VFO is a common feature of cerebral cortical oscillations (e.g., Cunningham et al., 2004; Traub et al., 2003). In these structures, the VFO appeared to be generated by nonsynaptic mechanisms, with evidence for involvement of gap-junction-mediated intercellular communication (Draguhn et al., 1998; Schmitz et al., 2001). Atypical feature of such rhythms is the presence of spikelets in participating neuronal subtypes. Depending on coupling efficacy, action potential generation in prejunctional neurons may generate either a subthreshold response or full action potentials in the postjunctional neuron. The subthreshold postjunctional potential change resembles a small version of the prejunctional full spike—the spikelet. Spikelets were observed during nicotine-induced cerebellar rhythms in 8/32 Purkinje cells in addition to full action potentials. Spikelets had a rise time of 0.3 ± 0.0 ms, half-width of 0.8 ± 0.0 ms, and a mean amplitude of 2.2 ± 0.1 mV (Figure 2B, Figure 3A, and Figure 3B, n = 7). In the Purkinje cells displaying spikelets, 35% ± 5% of all full action potentials recorded arose from spikelets (e.g., Figure 3A, right panel). Spikelet-triggered averaging demonstrated that both Purkinje and stellate cell spikelets were phase locked to negative-going VFO frequency field events (Figure 3C). Spikelets were never observed in Purkinje cells in nonoscillating conditions (0/23).

However, the pharmacology of VFO in cerebellum was different from that seen in other cortical regions. Here, the VFO was enhanced by $GABA_A$ receptor blockade (Figure 2A). Cerebellar molecular layer interneurons have been shown to be very densely, nonsynaptically interconnected (Mann-Metzer and Yarom, 1999; Van Der Giessen et al., 2006). If interneurons are also capable of participating in VFO, this may, in part, explain the effects of $GABA_A$ receptor blockade. We therefore looked for spikelets in interneurons during high-frequency oscillations induced by nicotine. Stellate cells, in the presence of nicotine, fired with a mean frequency of 38 ± 2 Hz (n = 5), with spike-triggered averaging demonstrating that firing was phase locked to the gamma frequency field rhythm (data not

shown). Hyperpolarization (5 mV from RMP) revealed the regular occurrence of spikelets at VFO frequencies in all cells (Figure 3A). These stellate cell spikelets had a mean amplitude of 2.6 ± 0.3 mV, a mean rise time of 0.3 ± 0.0 ms, and a mean half-width of 0.8 ± 0.0 ms (i.e., they were not significantly different in amplitude or kinetics from those seen in Purkinje cells, $p < 0.05$, $n = 5$). Spike-triggered averaging revealed that these spikelets were also phase locked to the nicotine-induced VFO rhythm (Figure 3Cii). However, alignment to band-pass-filtered gamma field potential rhythms revealed that spikelets, on average, preceded full spike generation by 3–8 ms (Figure 3C). Basket cells also displayed regular spikelets. Action potential rates were lower than those of stellate cells (10 ± 3 Hz, $n = 4$), but they tended to generate short bursts of gamma or VFO frequency action potentials separated by periods of relative quiescence (Figure 3A). In contrast to full action potential generation, spikelet generation was continuous and at VFO frequency. These events had an amplitude of 3.4 ± 0.2 mV, rise time of 0.9 ± 0.1 ms, and half-width of 2.0 ± 0.0 ms. Both rise time and half-widths of these spikelets were significantly slower than spikelets in both stellate and Purkinje cells ($p < 0.001$). In each cell type, spikelets were seen to give rise to full action potentials (Figure 3A), and spikelets were abolished by somatic hyperpolarization (Figure 3B).

The widespread presence of spikelets, and their temporal relation to the field VFO, suggested that nonsynaptic intercellular communication may play a role in generating this cerebellar rhythm. To test this, we abolished all phasic synaptic neurotransmitter release by removing calcium ions from the aCSF. In calcium-free conditions, no gamma frequency population rhythms were seen, but the VFO survived (Figure 4). To verify that no transmembrane calcium ion-mediated electrogenesis was present in these conditions during the VFO, we applied the main Purkinje cell calcium channel subtype (P/Q, Regan, 1991) blocker ω-agatoxin. No significant effect of P/Q channel blockade was seen on VFO rhythm area power (control power 2309 ± 227, with P/Q channel block 2497 ± 302 μV^2, $n = 6$, $p > 0.05$). In contrast, blockade of voltage-dependent sodium channels with TTX abolished the field VFO ($n = 6$, $p < 0.001$, Figure 4A). Reduction in intercellular gap-junction-mediated coupling with carbenoxolone (0.1 mM) also abolished the calcium-free population VFO ($p < 0.001$, $n = 6$). The population VFO seen in these conditions was also accompanied by regular trains of somatic spikelets in Purkinje cells (Figure 4B). As with spikelets seen during gammaA/VFO high-frequency rhythms, they were tightly phase locked to the negative peak of the concurrently recorded field potential rhythm (cf. Figure 4B with Figure 3C).

In addition to the widespread incidence of spikelets and survival of the VFO in the absence of calcium-mediated, phasic transmitter release, heterocellular dye coupling was prevalent in cerebellar cortical slices. In the presence of nicotine-induced field potential rhythms, 8/23 Purkinje cells filled with biocytin showed dye coupling to molecular and Purkinje cell layer inter-neurons (Figure 5A and 5B). Five of 23 Purkinje cells were coupled to basket cells, and 3/23 were coupled to one or more stellate cell. As with spikelet incidence, the presence of dye coupling appeared to be related to the presence of high-frequency population rhythms in the cerebellum. While 8/23 Purkinje cells showed dye coupling to interneurons with somata distal to the filled neuron, no dye coupling at all was seen in control conditions (normal aCSF, no population rhythms, $n = 0/23$, $p < 0.001$).

The correlation between spikelet incidence and dye coupling with the VFO, and the observation that this rhythm was present in the absence of any phasic synaptic transmitter release, suggested a possible role for gap junctions in forming the underlying nonsynaptic network generating this rhythm. No selective gap junction blockers exist that can be readily applied to networks of many thousands of cells simultaneously. We therefore examined the effects of a broad range of gap junction blockers with widely differing additional effects on intrinsic membrane conductances and their second-messenger-related systems (Figure 5C) in order to establish whether a convergence of effect could be seen. Carbenoxolone (200 μM) almost completely abolished both gamma and VFO rhythms. Mean gamma band and VFO area powers were significantly reduced from 1809 ±186 μV^2 and 3643 ± 261 μV^2 to 88 ± 19 μM^2 and 103 ± 28.3 μV^2, respectively ($p < 0.001$, n = 6, Figure 5C). Octanol (1 mM) significantly reduced gamma and VFO powers from 369 ± 35 μV^2 and 931 ± 103 μV^2 to 33 ± 7 μV^2 and 88 ± 9 μV^2, respectively ($p < 0.001$, n = 6). Quinine (at concentrations 10-fold lower than reported for effects on intrinsic conductances) also massively attenuated oscillatory activity ($p < 0.001$, n = 6, Figure 5C). Both meclofenamic acid and 2-APB also abolished peak modal power in the VFO band ($p < 0.001$, n = 6, Figure 5C). Thus, all drugs tested with gap-junction-blocking ability significantly reduced the power in not only the VFO frequency range but also in the gamma frequency range.

Anatomical Extent of High-Frequency Oscillations

In order to establish the spatial extent of both gamma and VFO rhythms, dual extracellular recordings were made longitudinally along the Purkinje cell layer. Cross-correlograms of the paired field data revealed extensive spatiotemporal interactions at gamma frequencies (Figure 6A, upper panel), whereas interactions at VFO frequencies (in the presence of nicotine and gaba-zine) were more spatially localized. Gamma synchrony, defined as the amplitude of the cross-correlogram at 0 ms, decreased by 8% ± 2% per 0.1 mm (n = 5). VFO synchrony decreased by 19% ± 3% per 0.1 mm, indicating that field potential rhythms could synchronize over distance significantly more effectively at gamma rather than VFO frequencies ($p < 0.05$, n = 5). Interlaminar extent of the rhythms was examined by placing a reference electrode in the proximal molecular layer and a second electrode at positions from cortical surface to white matter (Figure 6B). Peak power for gamma rhythms originated in the Purkinje cell layer, with a sharp phase reversal of the field potentials observed between the Purkinje cell and molecular layers. In contrast, VFO rhythms had a maximal power in the granule cell layer, with a phase reversal between the surface and molecular layers (see Discussion).

Field potentials reflect current densities, and their interpretation depends on circuit architecture. To monitor local average membrane potential responses directly and to obtain a more spatially accurate picture of rhythm distribution, voltage-sensitive dye recordings (Matsukawa et al., 2003) were combined with electrophysiology. Change in fluorescence (from the region of interest indicated in Figure 7A) and field potentials of nicotine-induced gamma rhythms showed a high degree of correlation, with the field potential data leading the optical signal by about 4 ms. Band-pass filtering the optical signal within the gamma range (20–50 Hz) revealed rhythmic changes in fluorescence signal particularly evident in the Purkinje cell layer (where the field potential was maximal [see Figure 6B]), but was also

evident in deep white matter—a location where no gamma rhythm could be seen in the field potential (Figure 7B, cf. Figure 6B, see Discussion). Band-pass filtering the optical signal at VFO frequencies in the presence of nicotine and gabazine (70–150 Hz) revealed rhythmic changes in fluorescence in the proximal granule cell layer, extending through the white matter. To further quantify the anatomical location of the rhythms, pooled power spectral peaks in the gamma and VFO bands (2 s epochs, n = 5) were calculated for each pixel group and plotted onto an idealized cerebellar cortical lobule (Figure 7C). With this approach, the Purkinje cell layer/white matter origins of the gamma frequency optical signal can be clearly compared to the granule cell layer/white matter origins of the VFO frequency optical signal.

Correlates with Human Cerebellar Rhythms

Some of the central effects of nicotine have been suggested to involve cerebellum (Kumari et al., 2003). We therefore used slices of normal human cerebellar cortex (n = 3, obtained as part of cerebellar biopsies) to test whether the above features of nicotine-induced high-frequency oscillations in mouse may also apply to human cerebellum. Nicotine (1–10 μM) generated persistent high-frequency oscillations robustly (Figure 8). There was an apparent concentration difference for generating peak oscillation power, with human cerebellar slices responding maximally at 2 μM (cf. mouse slice peak powers at 10 μM, Figure 1B). Modal peak frequencies compared favorably across species, with human gamma power peaking at 42 ± 3 Hz and VFO power peaking at 132 ± 6 Hz. These superficial similarities do not necessarily implicate similar underlying mechanisms, so we tested the effects of gabazine, which abolished gamma power but boosted VFO power in mice, and quinine, which abolished both components of the high-frequency oscillation—two observations that are not seen for high-frequency oscillations in other cortical areas. As with data from mouse slices, gabazine (1 μM) abolished modal peak activity in the gamma band (an 80% reduction, n = 2) while concurrently increasing VFO power (a 260% increase, n = 2) (Figure 8A). Similarly, quinine (0.1 mM) appeared to be as effective at abolishing all high-frequency rhythms in human cerebellar slices as it was in mouse slices (a 95% reduction in peak gamma band power and an 80% reduction in VFO power, n = 2) (Figure 8B).

DISCUSSION

The present data demonstrate mechanisms for the generation of high-frequency field potential rhythms in the cerebellar cortex. These cerebellar rhythms are tuned to the same frequency bands as high-frequency oscillations in other neocortical areas (Fisahn et al., 1998; Cunningham et al., 2004). However, while the high-frequency spectral profiles matched other cortical areas (gamma rhythms and VFO), had the same interdependence (Cunningham et al., 2004), and had a similar ability to time network outputs, the underlying mechanisms revealed a number of differences.

Of these differences, the nature of the primary network drive was most striking. Cholinergic receptor activation generates gamma rhythms in hippocampus (Fisahn et al., 1998), entorhinal cortex (Dickson et al., 2000), and neocortex (A. Roopun and M.A.W., unpublished data). In each of these regions, the cholinergic drive is provided primarily by muscarinic receptor activation (e.g., Fisahn et al., 2002). In cerebellar cortex, nicotinic

cholinoceptors mediated the network activation. However, the rhythms seen were not the result of activation of the classical α_7 and $\alpha_4\beta_2$ neuronal nicotinic receptors. The muscle relaxants pancuronium and D-tubocurarine reduced oscillatory power, and D-tubocurarine also blocks interneuronal excitation in cerebellum following nicotine pressure ejection (de la Garza et al., 1987). The cerebellum contains many nonclassical nAChRs. Turner and Kellar (2005) reported six structurally distinct heteromeric nAChR populations in the rat cerebellum, including several subtypes that had not been previously encountered. These data suggest that cerebellar high-frequency rhythms are generated by an as yet undefined nicotinic receptor subtype, with more homology to peripheral, rather than established central neuronal, types of receptor. Nicotinic receptors have been implicated in cerebellar dysfunction in autism (Martin-Ruiz et al., 2004), and elevated nicotine levels associated with cigarette smoking produce cerebellar tremor (Louis, 2007).

From a network dynamic perspective, the profile of gamma rhythms in cerebellar cortex was particularly intriguing. The rhythm did not require activation of AMPA, kainate, or NMDA receptors, indicating an absence of fast glutamatergic synaptic excitation in the underlying mechanism. This was in stark contrast to the critical role played by phasic synaptic excitation of interneurons in persistent gamma rhythms in other cortical areas (e.g., Whittington and Traub, 2003) where it is the recurrent inhibitory circuit, activated by excitatory outputs from the principal cell population, that provides the basic rhythm generator (Traub et al., 2000; Cunningham et al., 2004). Given that nicotine provides tonic excitation to molecular layer interneurons in cerebellar cortex (de la Garza et al., 1987) and that the principal cell population is also GABAergic, the gamma rhythms generated appeared to be similar to the ‘interneuron network gamma’ seen transiently in hippocampus and neocortex in nonphysiological conditions (glutamate receptors pharmacologically blocked; Whittington et al., 1995). The differences between this original demonstration of mutual inhibition-dependent gamma rhythm and the cerebellar gamma rhythm presented here were as follows. (1) The cerebellar rhythm was persistent—occurring as long as nicotine was present. (2) The active network has an “inverted” function for the principal cells—in cerebellum, principal cell outputs feed back to interneurons as part of the mutual inhibitory circuit. In addition, it appears that the field potential gamma rhythm required a heterogeneous GABAergic neuronal population—both Purkinje cell and local Interneuronal involvement was necessary. Purkinje cells generate gamma frequency outputs alone in control conditions, but this was not manifest as a local field potential rhythm, indicating that synchronizing factors (such as local circuit Interneuronal activity) were essential.

In the absence of local circuit synaptic excitation, it is surprising that precise local temporal order could be maintained within such a heterogeneous GABAergic neuronal population. Connectivity between GABAergic neurons using inhibitory synaptic connectivity alone is acutely sensitive to the degree of variance in tonic drives (Chow et al., 1998), and while interneurons were depolarized during cerebellar high-frequency rhythms, Purkinje cells were actually hyperpolarized. However, in neocortex, GABAergic interconnections are capable of establishing robust temporal order when connectivity is mixed—consisting of $GABA_A$ receptor-mediated inhibitory synaptic events and direct electrical coupling (Traub et al., 2001; Szabadics et al., 2001). A similar pattern of temporal control has been shown for cerebellar interneurons (Mann-Metzer and Yarom, 2002). During gamma/VFO rhythms,

coupling potentials were seen in all cell types examined in the present study (basket, Purkinje, and stellate) and were phase locked to the local field potential rhythm. It is interesting to note that Purkinje cell coupling potentials were extremely variable in amplitude compared to coupling potentials observed in other cortical principal cells. Preliminary modeling studies suggest that this is caused by the particular pattern of distribution of fast sodium conductances relative to sites of electrotonic intercellular conductances in this cell type (R.D.T., unpublished data).

Synchronous generation of coupling potentials can give rise to population VFO in cortical areas in the absence of synaptic inhibition (Traub et al., 2003) and persist in reduced extracellular calcium-containing media, indicating the nonsynaptic nature of the underlying network structure (Draguhn et al., 1998). These phenomenon were also observed in cerebellum (Figures 2 and 3). As in these previous studies, the cerebellar VFO field potential was maximal in laminae containing principal cell axons and was blocked by tetrodotoxin, suggesting that the rhythm may be formed by action potential spread through a plexus of nonsy-naptically connected axonal compartments (Traub et al., 2000). Somatic full spike generation was seen at a much lower rate than spikelet coupling potential generation. However, it has been demonstrated that these cells can initiate action potentials far along their axons (Clark et al., 2005), and voltage-sensitive dye recordings demonstrated intense VFO activity in white matter (Figure 8). Axonal action potentials at VFO frequency may fail to propagate fully back to soma in a manner dependent on perisomatic inhibition, perhaps accounting for the marked enhancement of VFO signal on blockade of $GABA_A$ receptors. The resulting VFO rhythm was highly locally synchronous but, in contrast to gamma rhythms, was not associated with synchrony over longer distances (Figure 6), suggesting that it may form a substrate for the discrete microcomplexes implicated in movement coordination (Apps and Garwicz, 2005).

The association of VFO with near ubiquitous spikelet coupling potential generation in all cells studied and the potentiation of both VFO and spikelets in the absence of any phasic synaptic transmitter release strongly suggest the existence of nonsynaptically coupled neuronal networks in cerebellar cortex. In hippocampus and neocortex, components of such networks can be revealed by patterns of dye coupling (Schmitz et al., 2001), and emergent activity can be blocked by drugs that reduce gap junction conductance. Unequivocal evidence for connexin-containing gap junctions between axons of principal cells forming such networks has recently been seen in hippocampus (Hamzei-Sichani et al., 2007). The strength of evidence for gap junctional involvement in cerebellar cortical nonsynaptic networks is not yet this good. Cerebellar cortical neurons express many subtypes of connexin (Belluardo et al., 2000; Teubner et al., 2000; Maxeiner et al., 2003; Van Der Giessen et al., 2006), and dye coupling between cerebellar cortical neurons can be very dense (Mann-Metzer and Yarom, 1999). The dye coupling between Purkinje cells and interneurons in the present study suggests that Purkinje cells may influence, and be recruited by, such nonsynaptic interneuron networks. There remains a possibility of Purkinje cell-Purkinje cell electrical and dye coupling. The differences in patterns of coupling potentials in Purkinje cells and interneurons suggest a different nonsynaptic network structure influencing the two cell types, but the only dye coupling evidence involves Purkinje cells

whose somatic membrane are directly juxtaposed (e.g., Figure 5B), a pattern that can be produced as artifact of the labeling procedure.

Many types of putative intercellular junction are present in cerebellar cortex (Sotelo and Llinas, 1972), of which conventional seven-layer gap junctions, known to facilitate dye and electrical coupling, are only a subset. The lack of specific gap-junction-blocking drugs also makes identification of the substrate for electrical and dye coupling difficult. However, five drugs that block gap junctions, but have widely differing secondary effects, all blocked VFO and their dependent gamma rhythm (Figure 5). Any effects of these drugs on synaptic transmission are unlikely to play a role in this blockade, as the VFO rhythm occurred in the absence of any phasic synaptic activity. It seems highly unlikely that their divergent effects on intrinsic membrane conductances may all, independently, lead to collapse of high-frequency oscillations, but this cannot yet be excluded.

The present data, along with that of Cunningham et al. (2004), suggest that interdependent, high-frequency oscillations in the gamma and VFO bands are generated in both neo- and cerebellar cortices by similar, though clearly not identical, mechanisms. Integration of sensory information by both structures is required to generate and coordinate motor commands with communication between the two areas occurring directly and indirectly (via pontine nuclei) in rodents (Ackerley et al., 2006; Odeh et al., 2005). Preliminary electrophysiological studies of high-frequency cerebellar rhythms in awake mice indicate a role for these rhythms in such cortico-cerebellar interactions (S.J.M., M.A.W., and T.K., unpublished data). Despite differences in cellular mechanisms underlying their generation, the frequency bands of the population rhythms are common in neocortex and cerebellum. This leads one to speculate that these discrete frequency bands not only serve to provide temporal coding of local circuit outputs but, when combined with spatial coding of somatosensory information, may also serve to provide a common temporal coding strategy for intercommunication between higher sensorimotor areas in the cerebellum and cerebrum.

EXPERIMENTAL PROCEDURES

Slice Preparation

Coronal sections (400 μm thick) of cerebellum containing crus I and II of the ansiform and paramedian lobules, structures with established connectivity with somatosensory neocortex (Tolbert, 1989), were prepared from adult male C57B/6 mice. All procedures conformed to the UK Home Office Animals (Scientific Procedures) Act 1986. Slices were further trimmed to separate the recording area (hemispheres) from the vermis and were maintained at the interface between artificial cerebrospinal fluid containing (in mM) NaCl, 126; KCI, 3; NaH_2PO_4, 1.25; $CaCl_2$, 2; $MgSO_4$, 1; $NaHCO_3$, 24; glucose, 10, and warmed, wetted 95% O_2/5% CO_2 at 35°C. For experiments with calcium-free artificial cerebrospinal fluid, calcium was omitted and $MgSO_4$ raised to 4 mM. The rhythmogenic, cholinergic compounds physostigmine (10 μM) and nicotine (2–20 μM) were bath applied alone or with cholinergic antagonists atropine (10 μM), d-tubocurarine (dTC, 10 μM), dihydro-β-erythroidine (DHE, 10 μM), chlorisondamine di-iodide (CAI, 10 μM), pancuronium (pan, 10 μM), or methyllylcaconitine (MLA, 10 μM). All drugs were obtained from Tocris Bioscience (UK).

Slices of human cerebellar cortex comprised normal tissue obtained during surgery for cerebellar biopsy or tumor removal. In all cases, human tissue was dissected from the paramedian lobule. Following surgical removal, tissue adjacent to the lesion was rapidly transferred to cooled aCSF (composition as above) and 400 μm sections containing all cortical laminae transferred to a standard interface chamber. All tissue was obtained with patient consent and with approval of South Tees Local Research Ethics Committee #06/Q1003/51), the Newcastle Upon Tyne Hospitals NHS Trust (#CM/PB/3707), and the Home Office (HTA#12164).

Electrophysiology

Field potential recordings and laminar profiles were obtained by using paired glass micropipettes (0.5–2 MΩ) filled with aCSF. Data were broadband filtered at 1 Hz to 20 kHz to assess both local field potential and multiunit activity. Multiunit activity was found to be highly locally synchronous, generating population spiking that was evident with more narrow low-pass filtering below 400 Hz. To optimize signal/noise ratios, data were therefore presented band-pass filtered in the range 1–400 Hz. Intracellular recordings (0–10 kHz) from Purkinje cells, stellate cells, and basket cells were obtained using glass pipettes (50–90 MΩ) filled with 2 M potassium methylsulphate and 1 % w/v biocytin for post hoc anatomical identification and assessment of dye coupling. Power spectra and correlograms were constructed using Matlab software and statistical analysis performed using paired t tests or Mann-Whitney tests on normally or nonnormally distributed data where appropriate, with significance set at $p < 0.05$.

Imaging

Cerebellar slices were prepared as described above, then stained with the voltage-sensitive dye di-4-ANEPPS (Molecular Probes, Eugene, OR; 5 μM prepared from a stock solution in ethanol/DMSO [2:1], diluted 200:1 in oxygenated ACSF) for 30 min and transferred to the recording chamber. The epifluorescence setup consisted of a 1.6× objective, a dichroic mirror (575 nm), a long-pass filter (590 nm), and an inverted 1.6× projection objective mounted above the slice. A 532 nm laser (Verdi; Coherent Inc., Palo Alto, CA) was used to generate fluorescence, which was imaged with a high-speed 100 × 100 pixel CCD camera (MiCAM ULTIMA, RIKEN, Japan) at 10 kHz. Data were 2 × 2 binned and filtered at 1 kHz before analysis in the Matlab environment.

Light Microscopy

Neurons were filled with biocytin (see above). At the end of the recording, slices were immersion fixed for 1–7 days in 4% paraformaldehyde in phosphate buffer solution (0.1 M, pH 7.2, PBS). Fixed slices were then gelatine-embedded and resectioned at 60 μm thickness. Sections were then processed using the avidin-biotinylated HRP complex reaction (Vectastain ABC Elite kit, Vector Laboratories, Peterborough, UK) with 0.05% 3,3°-diaminobenzidine tetrahydrochloride (DAB; Sigma, Poole, UK) as a chromogen to visualize the biocytin-filled neurons. The visualized neurons were then photographed with a standard light microscope (Leica, UK). Dye coupling was defined as the presence of a (by eye) equally dense biocytin reaction in neurons additional to the recorded neuron. Neurons with somata directly juxtaposed or superimposed onto the soma of the filled neuron were rejected

from the dataset. Numerous examples of incompletely filled (ghost) neurons, in addition to the directly filled neuron, were also rejected, owing to inability to confidently characterize these cell types.

Acknowledgments

We thank the Volkswagenstiftung and The Wolfson Foundation for supporting this work. We also thank M. Häusser, P. Chadderton, and the late E.H. Buhl for invaluable input at the beginning of this study.

REFERENCES

Ackerley R, Pardoe J, Apps R. A novel site of synaptic relay for climbing fibre pathways relaying signals from the motor cortex to the cerebellar cortical C1 zone. J. Physiol. 2006; 576:503–518. [PubMed: 16887878]

Apps R, Garwicz M. Anatomical and physiological foundations of cerebellar information processing. Nat. Rev. Neurosci. 2005; 6:297–311. [PubMed: 15803161]

Bauer M, Oostenveld R, Peeters M, Fries P. Tactile spatial attention enhances gamma-band activity in somatosensory cortex and reduces low-frequency activity in parieto-occipital areas. J. Neurosci. 2006; 26:490–501. [PubMed: 16407546]

Belluardo N, Mudo G, Trovato-Salinaro A, Le Gurun S, Charollais A, Serre-Beinier V, Amato G, Haefliger JA, Meda P, Condorelli DF. Expression of connexin36 in the adult and developing rat brain. Brain Res. 2000; 865:121–138. [PubMed: 10814742]

Canolty RT, Edwards E, Dalai SS, Soltani M, Nagarajan SS, Kirsch HE, Berger MS, Barbara NM, Knight RT. High gamma power is phase-locked to theta oscillations in human neocortex. Science. 2006; 313:626–628. [PubMed: 16888130]

Chow CC, White JA, Ritt J, Kopell N. Frequency control in synchronized networks of inhibitory neurons. J. Comput. Neurosci. 1998; 5:407–420. [PubMed: 9877022]

Clark BA, Monsivais P, Branco T, London M, Hausser M. The site of action potential initiation in cerebellar Purkinje neurons. Nat. Neurosci. 2005; 8:137–139. [PubMed: 15665877]

Cunningham MO, Whittington MA, Bibbig A, Roopun A, LeBeau FE, Vogt A, Monyer H, Buhl EH, Traub RD. A role for fast rhythmic bursting neurons in cortical gamma oscillations in vitro. Proc. Natl. Acad. Sci. USA. 2004; 101:7152–7157. [PubMed: 15103017]

de la Garza R, Bickford-Wimer PC, Hoffer BJ, Freedman R. Heterogeneity of nicotine actions in the rat cerebellum: an in vivo electrophysiologic study. J. Pharmacol. Exp. Ther. 1987; 240:689–695. [PubMed: 3806420]

Dickson CT, Biella G, de Curtis M. Evidence for spatial modules mediated by temporal synchronization of carbachol-induced gamma rhythm in medial entorhinal cortex. J. Neurosci. 2000; 20:7846–7854. [PubMed: 11027250]

Draguhn A, Traub RD, Schmitz D, Jefferys JG. Electrical coupling underlies high-frequency oscillations in the hippocampus in vitro. Nature. 1998; 394:189–192. [PubMed: 9671303]

Fisahn A, Pike FG, Buhl EH, Paulsen O. Cholinergic induction of network oscillations at 40 Hz in the hippocampus in vitro. Nature. 1998; 394:186–189. [PubMed: 9671302]

Fisahn A, Yamada M, Duttaroy A, Gan JW, Deng CX, McBain CJ, Wess J. Muscarinic induction of hippocampal gamma oscillations requires coupling of the M1 receptor to two mixed cation currents. Neuron. 2002; 33:615–624. [PubMed: 11856534]

Fries P. A mechanism for cognitive dynamics: neuronal communication through neuronal coherence. Trends Cogn. Sci. 2005; 9:474–480. [PubMed: 16150631]

Graham A, Court JA, Martin-Ruiz CM, Jaros E, Perry R, Volsen SG, Bose S, Evans N, Ince P, Kuryatov A, et al. Immunohistochemical localisation of nicotinic acetylcholine receptor subunits in human cerebellum. Neuroscience. 2002; 113:493–507. [PubMed: 12150770]

Gray CM, Konig P, Engel AK, Singer W. Oscillatory responses in cat visual cortex exhibit inter-columnar synchronization which reflects global stimulus properties. Nature. 1989; 338:334–337. [PubMed: 2922061]

Hamzei-Sichani F, Kamasawa N, Janssen WG, Yasumura T, Davidson KG, Hof PR, Wearne SL, Stewart MG, Young SR, Whittington MA, et al. Gap junctions on hippocampal mossy fiber axons demonstrated by thin-section electron microscopy and freeze fracture replica immunogold labeling. Proc. Natl. Acad. Sci. USA. 2007; 104:12548–12553. [PubMed: 17640909]

Harris KD, Csicsvari J, Hirase H, Dragoi G, Buzsaki G. Organization of cell assemblies in the hippocampus. Nature. 2003; 424:552–556. [PubMed: 12891358]

Jaarsma D, Ruigrok TJ, Caffé R, Cozzari O, Levey AI, Mugnaini E, Voogd J. Cholinergic innervation and receptors in the cerebellum. Prog. Brain Res. 1997; 114:67–96. [PubMed: 9193139]

Jones MS, Barth DS. Effects of bicuculline methiodide on fast (>200 Hz) electrical oscillations in rat somatosensory cortex. J. Neurophysiol. 2002; 88:1016–1025. [PubMed: 12163550]

Kopell N, Ermentrout GB, Whittington MA, Traub RD. Gamma rhythms and beta rhythms have different synchronization properties. Proc. Natl. Acad. Sci. USA. 2000; 97:1867–1872. [PubMed: 10677548]

Kumari V, Gray JA, Ffytche DH, Mitterschiffthaler MT, Das M, Zachariah E, Vythelingum GN, Williams SC, Simmons A, Sharma T. Cognitive effects of nicotine in humans: an fMRI study. Neuroimage. 2003; 19:1002–1013. [PubMed: 12880828]

Louis ED. Kinetic tremor: Differences between smokers and non-smokers. Neurotoxicology. 2007; 28:569–575. [PubMed: 17267044]

Mann-Metzer P, Yarom Y. Electrotonic coupling interacts with intrinsic properties to generate synchronized activity in cerebellar networks of inhibitory interneurons. J. Neurosci. 1999; 19:3298–3306. [PubMed: 10212289]

Mann-Metzer P, Yarom Y. Jittery trains induced by synaptic-like currents in cerebellar inhibitory interneurons. J. Neurophysiol. 2002; 87:149–156. [PubMed: 11784737]

Martin-Ruiz CM, Lee M, Perry RH, Baumann M, Court JA, Perry EK. Molecular analysis of nicotinic receptor expression in autism. Brain Res. Mol. Brain Res. 2004; 123:81–90. [PubMed: 15046869]

Matsukawa H, Wolf AM, Matsushita S, Joho RH, Knöpfel T. Motor dysfunction and altered synaptic transmission at the parallel fiber-Purkinje cell synapse in mice lacking potassium channels Kv3.1 and Kv3.3. J. Neurosci. 2003; 23:7677–7684. [PubMed: 12930807]

Maxeiner S, Kruger O, Schilling K, Traub O, Urschel S, Willecke K. Spatiotemporal transcription of connexin45 during brain development results in neuronal expression in adult mice. Neuroscience. 2003; 779:689–700. [PubMed: 12809690]

Niedermeyer E. The electrocerebellogram. Clin. EEG Neurosci. 2004; 35:112–115. [PubMed: 15164822]

Odeh F, Ackerley R, Bjaalie JG, Apps R. Pontine maps linking somatosensory and cerebellar cortices are in register with climbing fiber somatotopy. J. Neurosci. 2005; 25:5680–5690. [PubMed: 15958734]

Palva JM, Palva S, Kaila K. Phase synchrony among neuronal oscillations in the human cortex. J. Neurosci. 2005; 25:3962–3972. [PubMed: 15829648]

Quik M, Polonskaya Y, Gillespie A, Jakowec M, Lloyd GK, Langston JW. Localization of nicotinic receptor subunit mRNAs in monkey brain by in situ hybridization. J. Comp. Neurol. 2000; 425:58–69. [PubMed: 10940942]

Regan LJ. Voltage-dependent calcium currents in Purkinje cells from rat cerebellar vermis. J. Neurosci. 1991; 77:2259–2269. [PubMed: 1712382]

Schmitz D, Schuchmann S, Fisahn A, Draguhn A, Buhl EH, Petrasch-Parwez E, Dermietze IR, Heinemann U, Traub RD. Axo-axonal coupling, a novel mechanism for ultrafast neuronal communication. Neuron. 2001; 37:831–840. [PubMed: 11567620]

Shin SL, De Schutter E. Dynamic synchronization of Purkinje cell simple spikes. J. Neurophysiol. 2006; 96:3485–3491. [PubMed: 16987931]

Sotelo C, Llinas R. Specialized membrane junctions between neurons in the vertebrate cerebellar cortex. J. Cell Biol. 1972; 53:271–289. [PubMed: 4537207]

Soteropoulos DS, Baker SN. Cortico-cerebellar coherence during a precision grip task in the monkey. J. Neurophysiol. 2006; 95:1194–1206. [PubMed: 16424458]

Szabadics J, Lorincz A, Tamás G. Beta and gamma frequency synchronization by dendritic gabaergic synapses and gap junctions in a network of cortical interneurons. J. Neurosci. 2001; 27:5824–5831. [PubMed: 11466454]

Szurhaj W, Bourriez JL, Kahane P, Chauvel P, Mauguiere F, Derambure P. Intracerebral study of gamma rhythm reactivity in the sensorimotor cortex. Eur. J. Neurosci. 2005; 27:1223–1235. [PubMed: 15813932]

Tecchio F, Graziadio S, Barbati G, Sigismondi R, Zappasodi F, Porcaro C, Valente G, Balsi M, Rossini PM. Somatosensory dynamic gamma-band synchrony: a neural code of sensorimotor dexterity. Neuroimage. 2007; 35:185–193. [PubMed: 17234434]

Teubner B, Degen J, Sohl G, Guldenagel M, Bukauskas FF, Trexler EB, Verselis VK, De Zeeuw CI, Lee CG, Kozak CA, et al. Functional expression of the murine connexin 36 gene coding for a neuron-specific gap junctional protein. J. Membr. Biol. 2000; 176:249–262. [PubMed: 10931976]

Timofeev I, Steriade M. Fast (mainly 30–100 Hz) oscillations in the cat cerebellothalamic pathway and their synchronization with cortical potentials. J. Physiol. 1997; 504:153–168. [PubMed: 9350626]

Tolbert DL. Somatotopically organized transient projections from the primary somatosensory cortex to the cerebellar cortex. Brain Res. Dev. Brain Res. 1989; 45:113–127. [PubMed: 2917405]

Traub RD, Whittington MA, Stanford IM, Jefferys JG. A mechanism for generation of long-range synchronous fast oscillations in the cortex. Nature. 1996; 383:621–624. [PubMed: 8857537]

Traub RD, Bibbig A, Fisahn A, LeBeau FE, Whittington MA, Buhl EH. A model of gamma-frequency network oscillations induced in the rat CA3 region by carbachol in vitro. Eur. J. Neurosci. 2000; 12:4093–4106. [PubMed: 11069606]

Traub RD, Kopell N, Bibbig A, Buhl EH, LeBeau FE, Whittington MA. Gap junctions between interneuron dendrites can enhance synchrony of gamma oscillations in distributed networks. J. Neurosci. 2001; 21:9478–9486. [PubMed: 11717382]

Traub RD, Cunningham MO, Gloveli T, LeBeau FE, Bibbig A, Buhl EH, Whittington MA. GABA-enhanced collective behavior in neuronal axons underlies persistent gamma-frequency oscillations. Proc. Natl. Acad. Sci. USA. 2003; 100:11047–11052. [PubMed: 12960382]

Turner JR, Kellar KJ. Nicotinic cholinergic receptors in the rat cerebellum: multiple heteromeric subtypes. J. Neurosci. 2005; 25:9258–9265. [PubMed: 16207885]

Whittington MA, Traub RD, Jefferys JG. Synchronized oscillations in interneuron networks driven by metabotropic glutamate receptor activation. Nature. 1995; 373:612–615. [PubMed: 7854418]

Van Der Giessen RS, Maxeiner S, French PJ, Willecke K, Zeeuw CI. Spatiotemporal distribution of Connexin45 in the olivocerebellar system. J. Comp. Neurol. 2006; 495:173–184. [PubMed: 16435305]

Whittington MA, Traub RD. Interneuron diversity series: inhibitory interneurons and network oscillations in vitro. Trends Neurosci. 2003; 26:676–682. [PubMed: 14624852]

Womelsdorf T, Schoffelen JM, Oostenveld R, Singer W, Desimone R, Engel AK, Fries P. Modulation of neuronal interactions through neuronal synchronization. Science. 2007; 376:1609–1612. [PubMed: 17569862]

Yeh JJ, Yasuda RP, Davila-Garcia MI, Xiao Y, Ebert S, Gupta T, Kellar KJ, Wolfe BB. Neuronal nicotinic acetylcholine receptor tx3 subunit protein in rat brain and sympathetic ganglion measured using a sub-unit-specific antibody: regional and ontogenic expression. J. Neurochem. 2001; 77:336–346. [PubMed: 11279289]

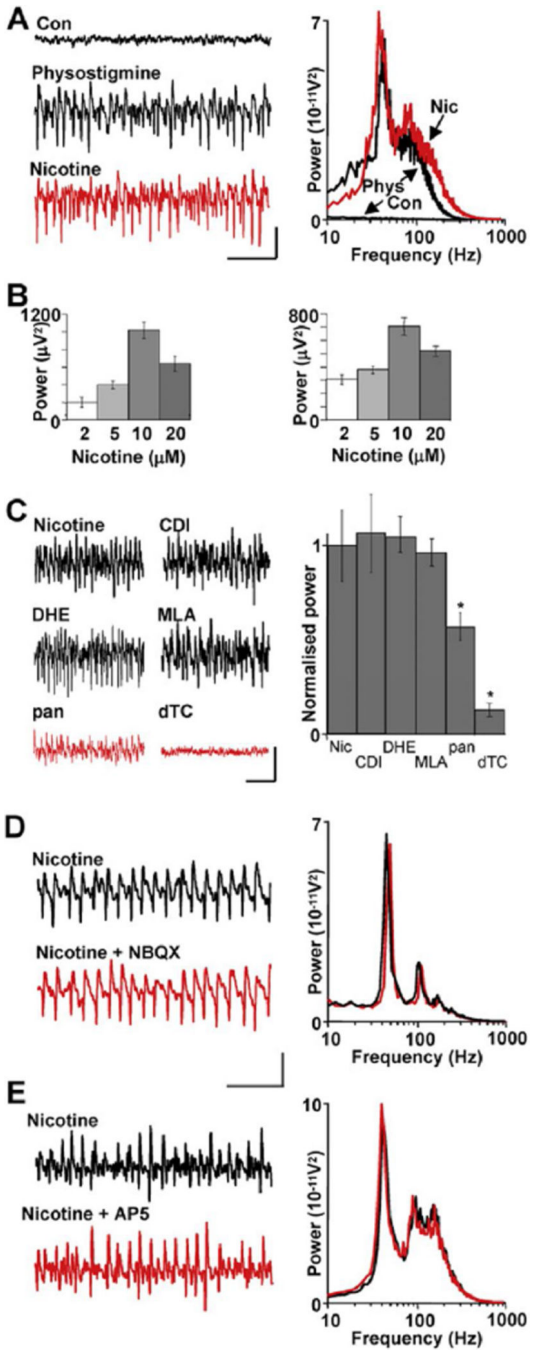

Figure 1. High-Frequency Oscillations Are Induced by Nicotinic Receptor Activation and Do Not Require Ionotropic Glutamate Receptors

(A) Enhanced levels of endogenous acetylcholine with physostigmine (10 μM) generate concurrent gamma and VFO rhythms. Example traces show data from a field electrode in the Purkinje cell layer. The spectrum of frequencies generated by physostigmine (black line) was reproduced by nicotine (10 μM) alone (red line). Scale bars: 0.1 mV, 100 ms.

(B) Concentration response for nicotine on gamma rhythms (left) and VFO (right). Note that maximal power in either band was obtained with 10 μM nicotine.

(C) Pharmacology of nicotinic response. Classical central neuronal nicotinic receptor subtype blockers (chlorisondamine diiodide [CDI], dihydro-β-erythroidine hydrobromide [DHE], methyllycaconitine citrate [MLA]—all bath applied at 10 μM) had no effect on the rhythms. However, the broad-spectrum nicotinic receptor antagonist d-tubocurarine (dTC) and the neuromuscular junction nicotinic receptor antagonist pancuronium (pan) significantly attenuated the rhythms (*$p < 0.05$). Scale bars: 0.1 mV, 100 ms.

(D) Lack of effect of bath application of NBQX (10 μM). Example traces are field potential recordings from the Purkinje cell layer. Spectrograms are pooled from n = 5 sets of 60 s data epochs, black lines control (nicotine alone), red lines nicotine and NBQX. Scale bars: 0.1 mV, 100 ms.

(E) Lack of effect of bath application of AP5 (50 μM).

Scale bars in (C) and (D): 0.1 mV, 100 ms. All data in bar graphs plotted as mean ± SEM.

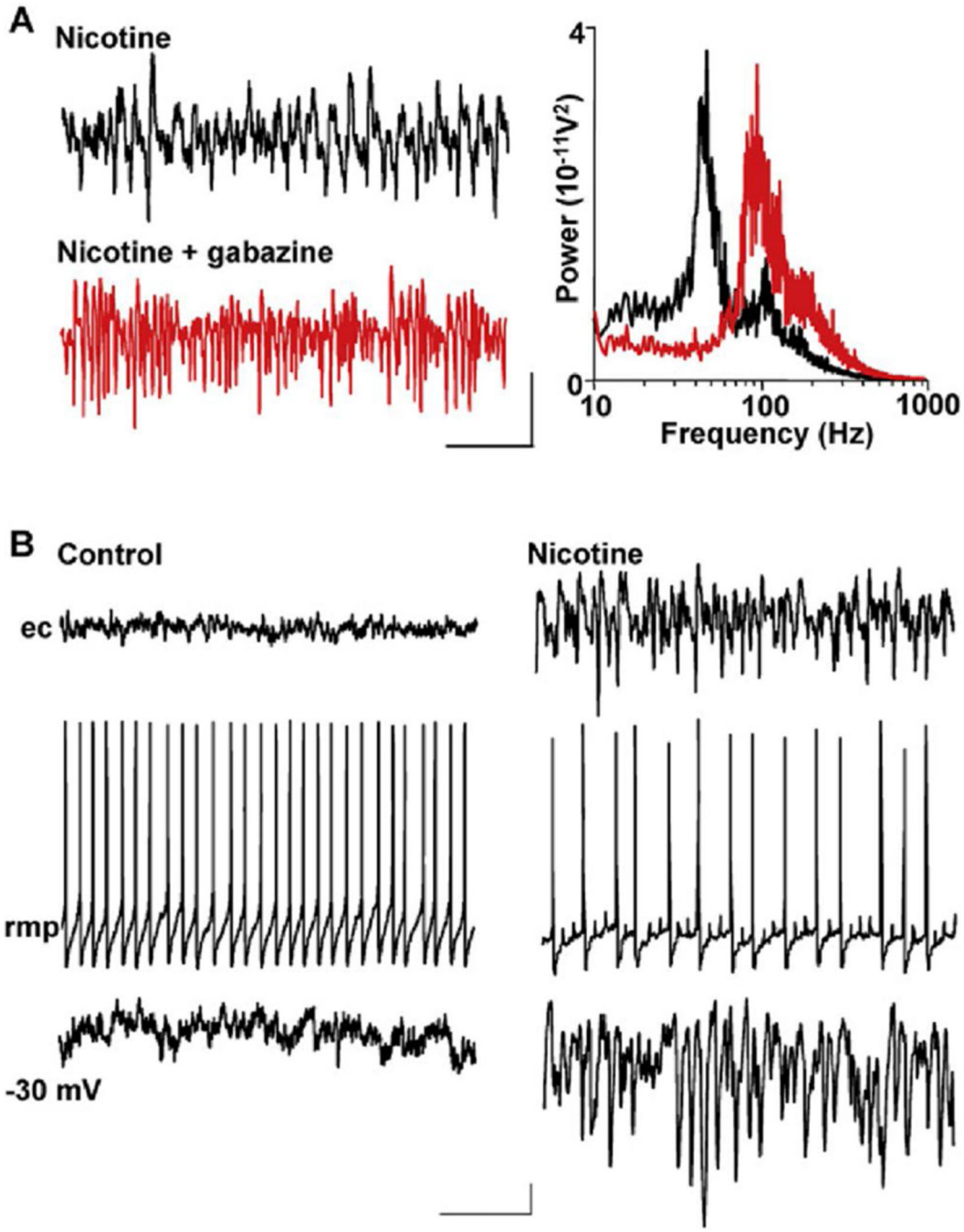

Figure 2. $GABA_A$ Receptor Activation Is Critical for Gamma Generation but Not VFO Generation

(A) Gabazine (1 μM) abolishes gamma rhythms but enhances VFO in field recordings. Example traces are field recordings from the Purkinje cell layer. Note the attenuation of gamma frequency activity and the predominance of VFO activity on blockade of $GABA_A$ receptors. Spectrograms are taken from 60 s epochs of field data (n = 5): black line, data in the presence of nicotine alone; red line, nicotine and gabazine. Scale bars: 0.1 mV, 100 ms. (B) Purkinje cell responses to nicotine application show gamma frequency inhibitory postsynaptic potentials. When bathed in aCSF alone, no rhythmic activity was seen in field

potential recordings, despite continuous action-potential generation in individual Purkinje cells (left panel). The Purkinje cell shown has a mean rmp of 58 mV. When depolarized to 30 mV by current injection, only very few, small IPSPs were seen. Scale bars: 50 μV (field), 10 mV (rmp), 2 mV (30 mV), 100 ms. In the presence of nicotine (right panel), Purkinje cell layer field potentials showed high-frequency oscillatory activity and individual Purkinje cells hyperpolarized by 4 mV. Purkinje cell spike rates were approximately halved, and multiple partial spikes (spikelets) were seen. Mean membrane potential of the Purkinje cell shown was 62 mV. Depolarization to 30 mV exposed intense trains of IPSPs at gamma frequency, phase locked to the field potential rhythm. Scale bars are as in the left panel.

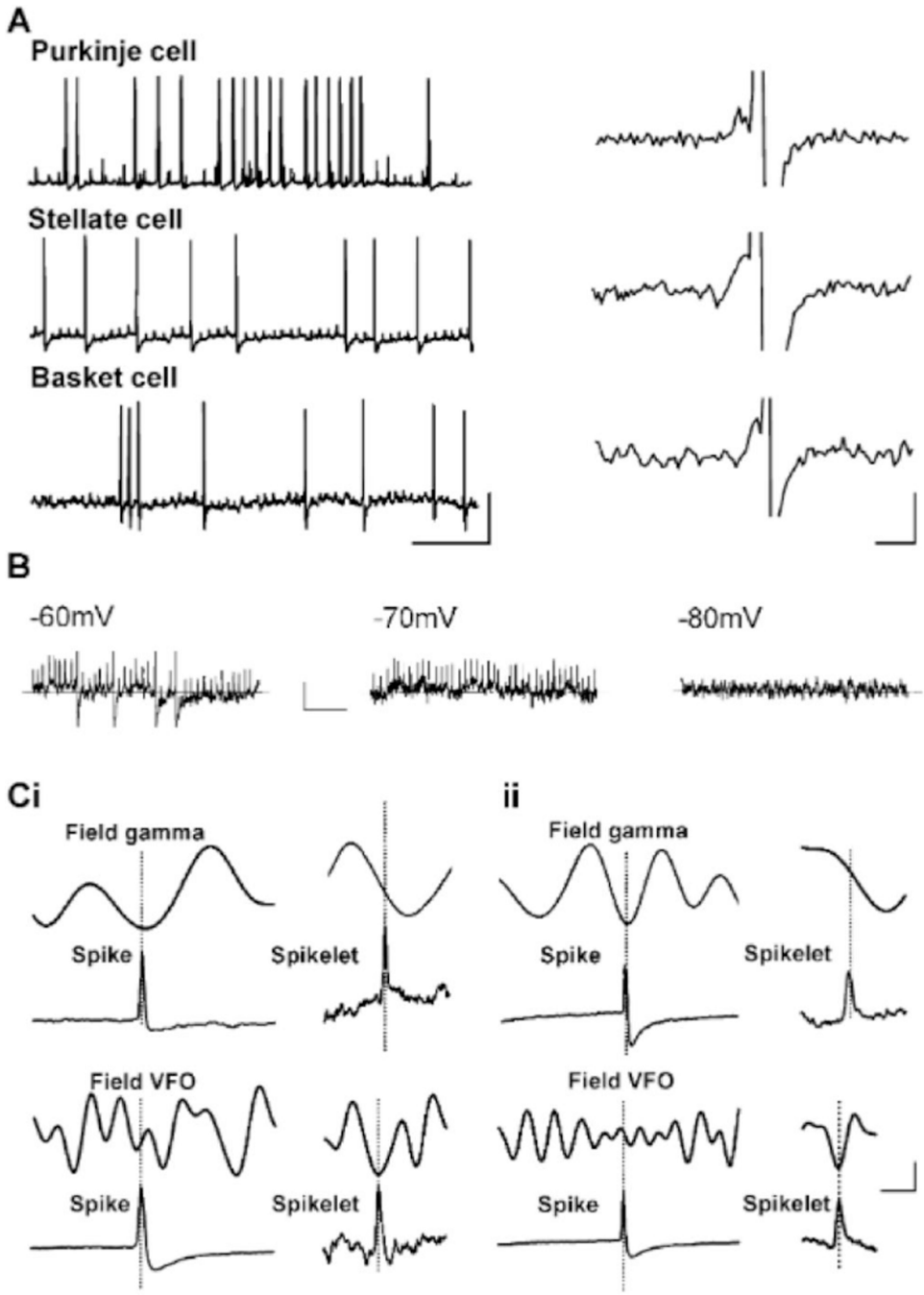

Figure 3. Pattern of Spikelet Generation during High-Frequency Oscillations

(A) Spikelets and antidromically elicited full spikes are seen in Purkinje cells and GABAergic interneurans during nicotine-induced rhythms. Example traces show somatic intracellular recordings from a Purkinje cell, a stellate cell in the molecular layer, and a basket cell in the Purkinje cell layer. Purkinje cells show clusters of spikelets at gamma frequencies (see also Figure 2B), while both interneurons generate single spikelets at VFO frequencies. Each cell type also generates occasional full action potentials, the majority of

which appear to arise from spikelets (examples in right panel). Scale bars: (left panel) 25 mV, 100 ms, (right panel) 5 mV, 3 ms.
(B) Stellate cell spikelets shown at progressively more hyperpolarized membrane potentials. Note that with sufficient hyperpolarization spikelet generation ceases—this was true for all recorded spikelets. Scale bars: 5 mV, 50 ms. (Ci) Purkinje cell spikes and spikelets are differentially phase locked to gamma and VFO field potential rhythms. Full-spike-triggered average of field potential (50 full spikes in n = 10 cells) revealed that full spikes fire at the trough of the concurrently recorded gamma frequency population potential (upper panel, field band-pass filtered at 30–80 Hz), but are poorly phase locked to VFO population rhythms (lower panel, field high-pass filtered at >80 Hz). In contrast, spikelet-triggered average (100 spikelets in n = 5 cells) revealed that spikelets fire in the trough of the field potential VFO (lower right panel) but are aligned to the descending phase of the gamma rhythm (upper panel). Scale bars: 20 μV (field average), 25 mV (intracellular full spike average), 5 ms. (Cii) Equivalent timing data for stellate cell action-potential firing with respect to gamma frequency field events (100 full spikes in n = 5 cells). Note that for both cell types action potentials are phase locked to the gamma frequency oscillation, while spikelets are phase locked to VFOs. Scale bars as in (Ci).

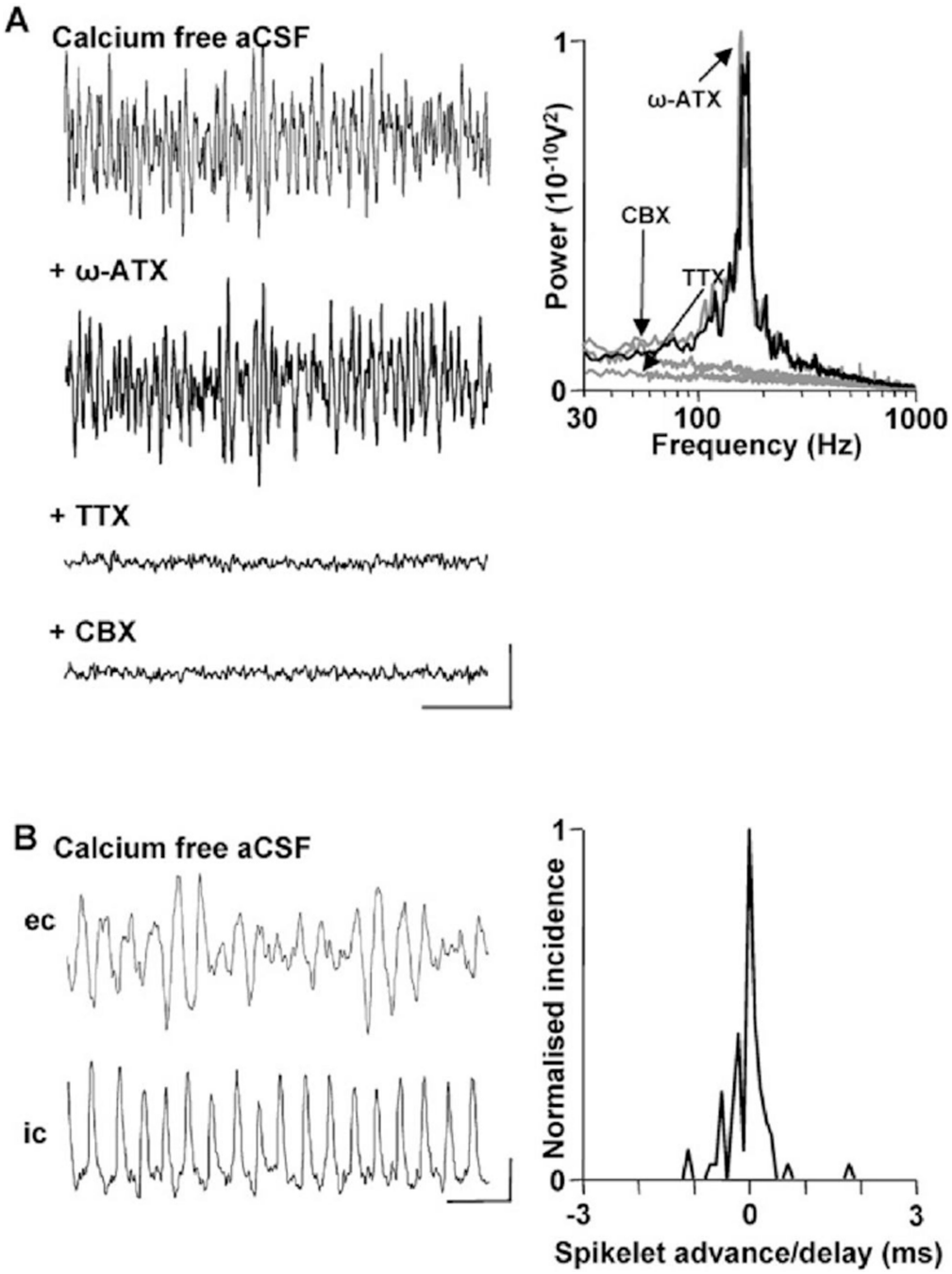

Figure 4. VFO and Spikelets, but Not Gamma Rhythms, Survive in Calcium-Free Extracellular Medium

(A) Blockade of phasic transmitter release via removal of calcium ions from the extracellular bathing solution (aCSF) abolished gamma frequency population oscillations but did not affect the VFO. Blockade of the main transmembrane calcium channels in Purkinje cells with ω-agatoxin (ω-ATX, 100 nM) had no effect on calcium-free VFO. However, blockade of fast sodium channels with tetrodotoxin (TTX, 100 nM) abolished population VFO rhythms. Bath application of the broad-spectrum gap junction blocker carbenoxolone (CBX, 0.1 mM) also abolished population rhythms. Scale bars: 0.2 mV, 50 ms.

(B) Population VFO was accompanied by phase-locked trains of spikelets in individual Purkinje cells. Traces show concurrently recorded somatic Purkinje cell response and local field potential VFO. Graph shows tight temporal correlation between spikelet peak and the trough of the corresponding field potential VFO, cf. Figure 3C (n = 200 spikelets from n = 5 Purkinje cells). Scale bars: 0.2 mV (field), 2 mV (intracellular), 10 ms.

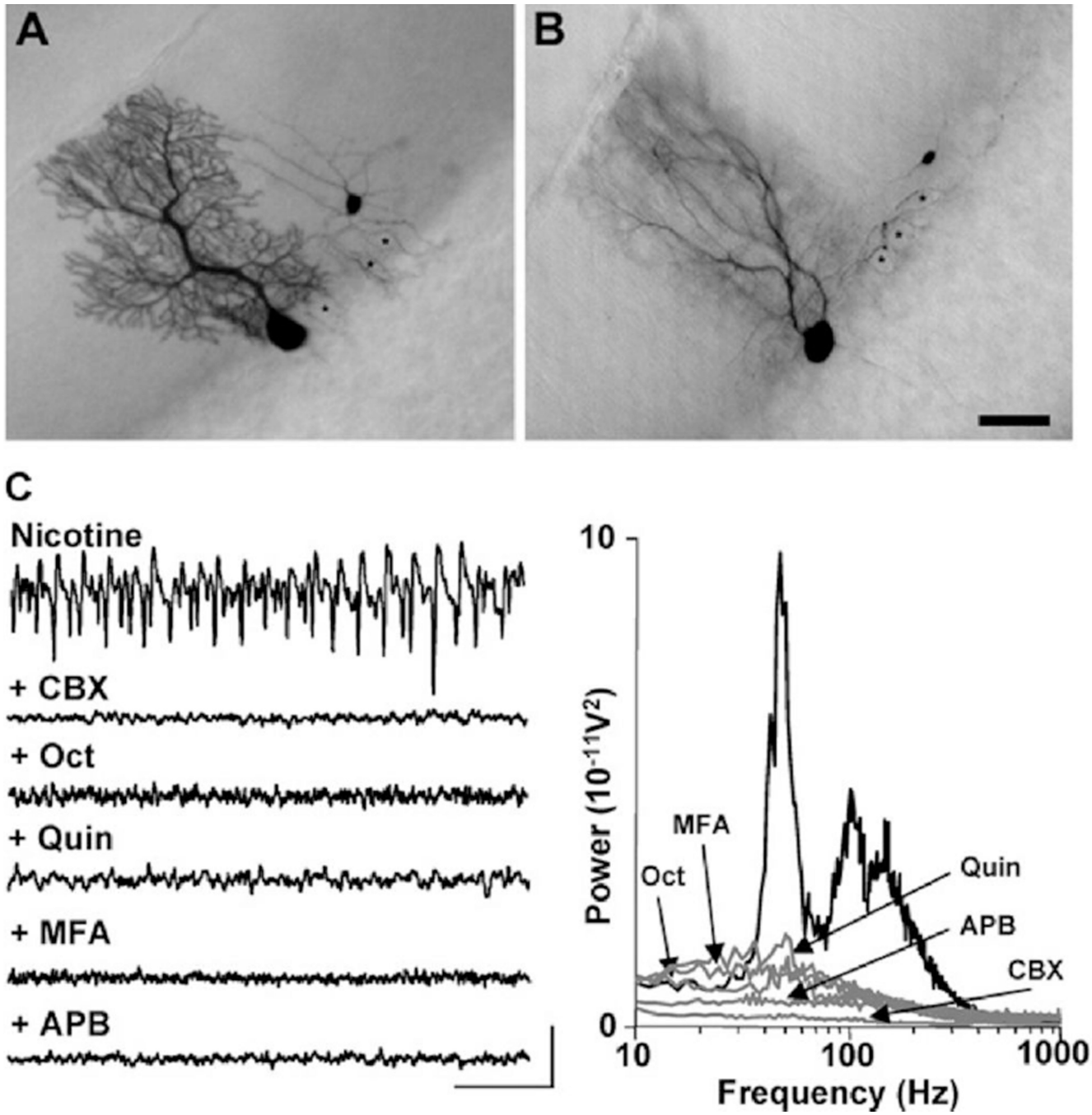

Figure 5. Heterocellular Dye Coupling and Sensitivity to Gap Junction Blockers Occur during High-Frequency Oscillations

(A and B) Examples of filled neurons following biocytin injection in a single, electrophysiologically identified Purkinje cell. The dye filling of the soma of the basket cell is likely to occur via the cell processes, as somata were clearly separate. The basket cell axon forms a basket around the soma of the filled Purkinje cell, as well as those of various unfilled Purkinje cells (asterisk). In (B), two superimposing Purkinje cells were labeled (note the two dendritic trees). Scale bar: 20 μm.

(C) Both gamma rhythms and VFO are sensitive to a range of gap-junction-blocking drugs. Unlike $GABA_A$ receptor blockade (Figure 2), drugs reducing gap-junction conductance blocked *both* gamma rhythms and VFO. Upper trace shows Purkinje cell layer field recording in the presence of nicotine. Traces below show effects of a mixture of nicotine and carbenoxolone (CBX, 0.2 mM), octanol (Oct, 1 mM), quinine (Quin, 0.01 mM), meclofenamic acid (MFA, 50 μM), and 2-APB (APB, 50 μM). Scale bars: 0.1 mV, 100 ms. Graph shows pooled power spectra (n = 6, 60 s epochs) for each of the above conditions.

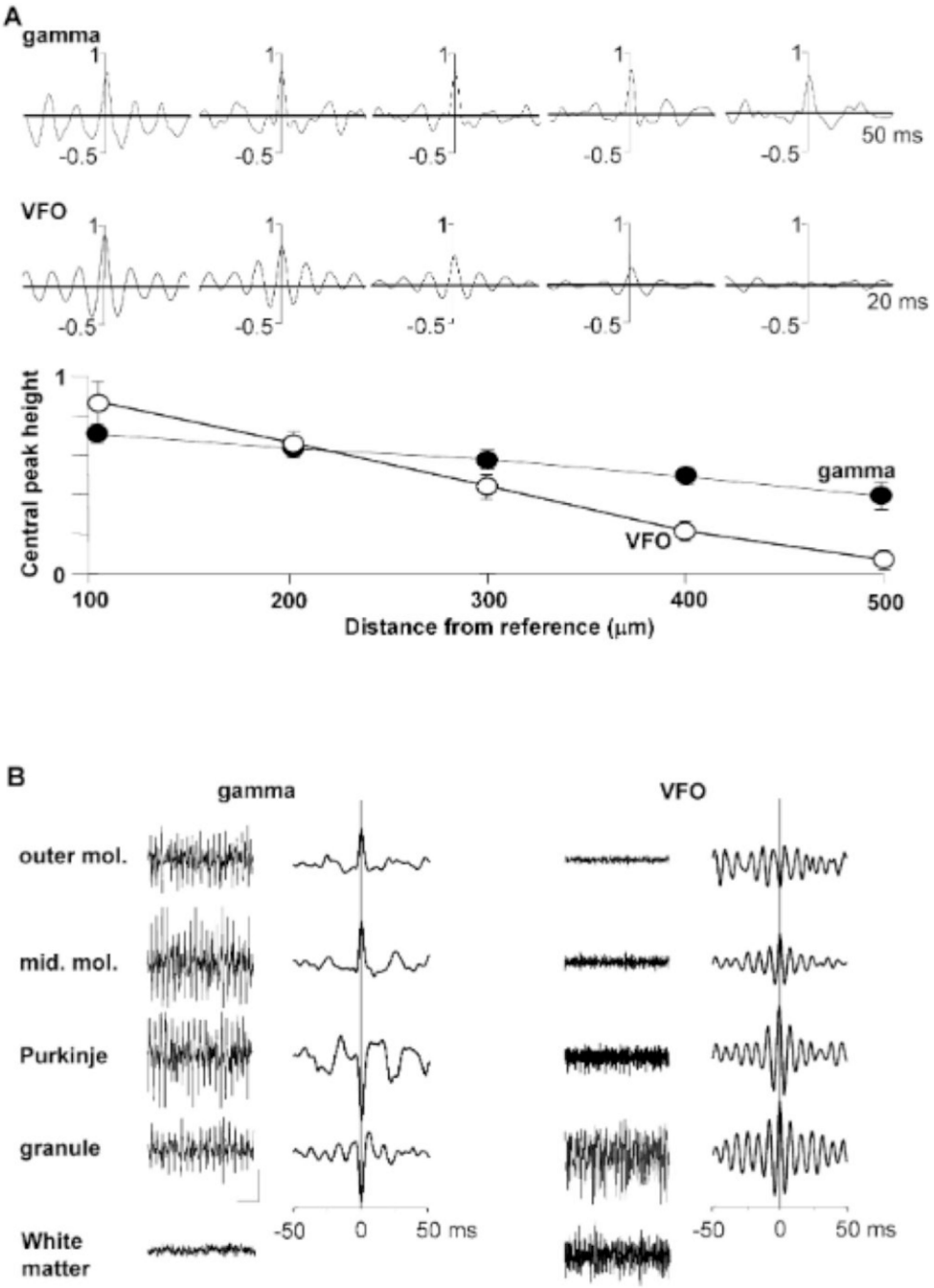

Figure 6. Inter- and Intralaminar Distribution of High-Frequency Oscillations

(A) Spatial extent of oscillations along the Purkinje cell layer. Cross-correlograms show pooled data (2 s epochs, n = 5 slices) comparing field rhythms recorded from the Purkinje cell layer with two electrodes at distances between 100 to 500 μm. Upper correlograms show data from slices bathed in nicotine alone. Lower traces show data from slices bathed in nicotine and gabazine. Lower graph shows the height of the cross-correlogram at 0 ms from all experiments (mean ± SEM) for rhythms where the modal spectral peak was at gamma frequencies (filled symbols) and VFO frequencies (in the presence of gabazine, unfilled

symbols). Note the 2-fold greater drop in synchrony at VFO frequencies with distance along the Purkinje cell layer.

(B) Laminar profile of high-frequency oscillations. Example traces show field potential activity in the presence of nicotine (left panel, gamma) and nicotine + gabazine (right panel, VFO). Recording electrodes were placed in the outer and mid molecular layers (outer mol., mid. mol.), Purkinje cell layer, granule cell layer, and white matter. Graphs show cross-correlations between electrodes at these locations and a reference electrode in the inner molecular layer. Note that the phase reversal for gamma rhythms is located at the Purkinje cell layer, whereas that for VFO is in the distal dendritic field. Note also the absence of electrophysiological evidence for gamma rhythms in the white matter, whereas the VFO signal is still very strong. Scale bars: 0.1 mV, 100 ms.

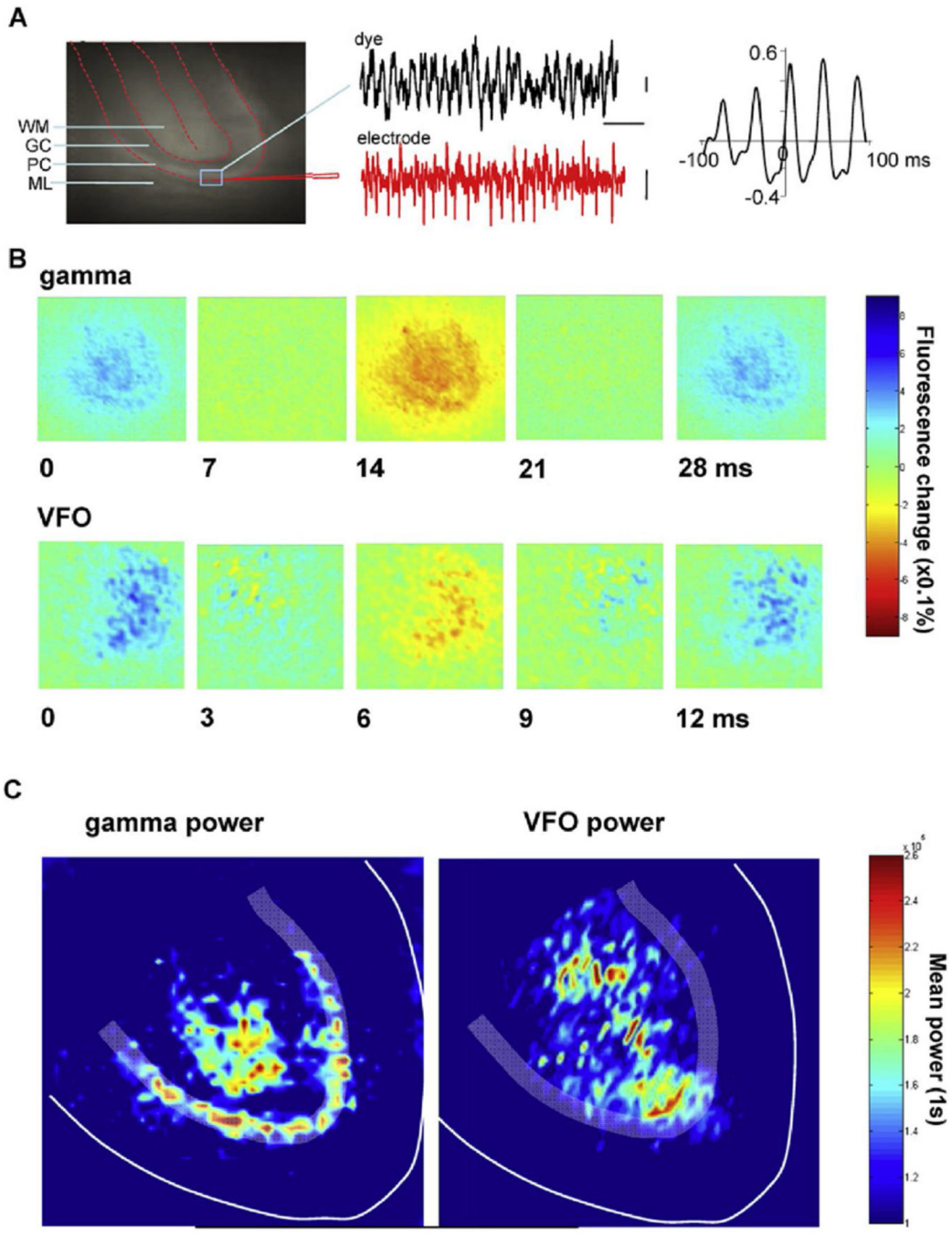

Figure 7. Optical Recordings Show Differential Origin of Gamma Rhythms and VFO

(A) Comparison of electrophysiology and voltage-sensitive dye recordings. Fluorescence image of a dye-stained cerebellar slice with indication of the main anatomical features (WM, white matter; GC, granule cell layer; PC, Purkinje cell layer; ML, molecular layer) and the location of an extracellular field electrode and overlaid region of interest for fluorescence signal. Example traces show concurrent field and dye recordings of high-frequency oscillations induced by nicotine. Graph shows cross-correlation between electrophysiology

and dye data. Note the overt rhythmicity at gamma frequencies and the slight phase lag of optical versus electrophysiological data.

(B) Example frames from two recordings showing the spatial extent of the fluorescence signal change during one gamma period (nicotine, upper panels) and one VFO period (nicotine + gabazine, lower panels). Frame times (in millisecond) are shown from the peak positivity in the dye signal for one period.

(C) Pooled peak power in the gamma band (20–60 Hz) and VFO band (80–160 Hz) from power spectra of the optical data (n = 5, 1 s epochs) morphed onto an idealized lobule slice. Note that peak gamma power is mainly confined to the Purkinje cell layer around the apex of the lobule, but with additional signal in the gamma band in distal white matter. In contrast, VFO peak power was seen in the granule cell layer at the lobule apex and diffusely in white matter. Images taken were from 2.5 × 2.5 mm regions of cerebellar slice, 50 × 50 (2 × 2 binned) pixels.

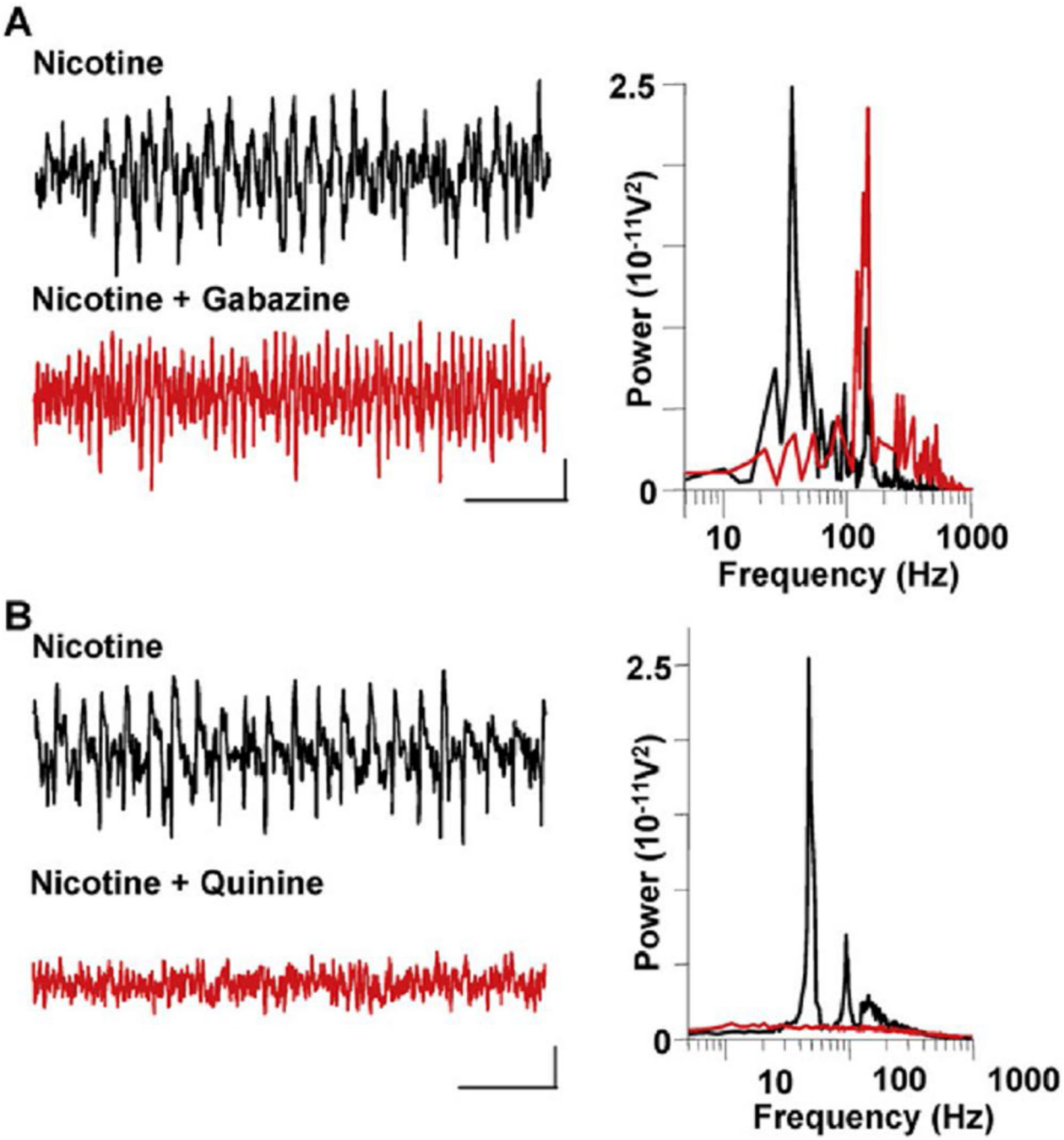

Figure 8. Nicotine-Induced High-Frequency Oscillations in Human Cerebellar Cortex

(A) Gamma rhythms and VFO are generated in human cerebellar cortex slices by 2 μM bath application of nicotine. Example traces show field potential recordings from the Purkinje cell layer in the presence of nicotine alone (upper trace) and nicotine + gabazlne (1 μM, lower trace). Power spectra for these two conditions are shown (n = 2, 60 s data epochs). Scale bars: 0.05 mV, 100 ms.

(B) Both gamma rhythms and VFO In human cerebellar slices were abolished by quinine (0.1 mM). Scale bars: 0.05 mV, 100 ms.